

Performance optimization of Nernst-based thermionic engines

Wei Yan^{1,*}, Minglong Lv^{1,*}, Ousi Pan¹, Zhimin Yang², Jincan Chen¹, and Shanhe Su^{1†}

¹*Department of Physics, Xiamen University, Xiamen 361005, People's Republic of China*

²*School of Physics and Electronic Information, Yan'an University, Yan'an 716000, People's Republic of China*

(Dated: April 10, 2025)

In this paper, we examine the power and efficiency of the thermionic device utilizing the Nernst effect, with a specific focus on its potential application as an engine. The device operates by utilizing the vertical heat current to generate a horizontal particle current against the chemical potential. By considering the influence of a strong magnetic field, we derive analytical expressions for the current and heat flux. These expressions are dependent on the temperature and chemical potential of heat reservoirs, providing valuable insights into the device performance. The impact of driving temperatures on the performance of the thermionic engine has been assessed through numerical analysis. The research findings will guide the experimental design of Nernst-based thermionic engines.

The Nernst effect refers to a thermoelectric or thermomagnetic phenomenon that is observed in electrically conductive materials when subjected to perpendicular magnetic field and temperature gradient [1–3]. This phenomenon is a result of charge carriers diffusing in response to the magnetic field, generating a transverse electric field that is directly proportional to the applied temperature gradient.

The Nernst effect has primarily been studied and observed in metallic and semiconducting materials [4–8]. It has applications in various areas, such as thermoelectric devices, spintronics, and energy harvesting. Sothmann theoretically proposed Nernst engines based on quantum Hall edge states, where they are identified to have the performance surpassing classical counterparts [9]. Graphene, with its distinctive electronic and thermal properties, has also garnered significant attention in the investigation of the Nernst effect [10]. The presence of a magnetic field perpendicular to the graphene sheet can give rise to intriguing transport phenomena attributable to the quantum Hall effect and the Landau quantization of electronic states. Bergman proposed a theory of conductivity that is expressed in terms of entropy per carrier, offering valuable insights into the characteristics of Nernst thermopower in two-dimensional graphene materials [11]. Sharapov provided an insightful visualization of the Nernst effect in Laughlin geometry by employing an ideal reversible thermodynamic cycle [12]. Investigation on the reduction of magnetic field intensity has revealed an enhanced spin Nernst effect, which demonstrates sensitivity to both sample characteristics and contacts [13]. In addition, the unique characteristic of the anomalous Nernst effect, which does not depend on a strong magnetic field, has attracted significant attention in various ferromagnetic materials [14–19].

It is crucial to emphasize that the practical realization of the classical Nernst engine faces significant challenges that need to be addressed [20, 21]. Firstly, the

existing devices suffer from low efficiency, which severely limits their power generation capability. Moreover, the implementation of magnetic fields in practical settings requires some cost. Under these circumstances, a structure for generating thermoelectric energy via the ordinary Nernst effect in the absence of an external magnetic field has been proposed [22]. A simplified model has been proposed for an engine that harnesses the Nernst effect. This model revolves around the migration of electrons between four heat reservoirs operating at different temperatures [23, 24] and encompasses the transport of heat and particles in non-interacting systems, drawing an analogy to the Landauer-Büttiker approach [25]. In this study, we extensively delve into the theoretical framework, providing comprehensive expressions for current and heat flow within the classical Nernst engine. Furthermore, we conduct thorough calculations to determine the power and efficiency of the Nernst engine under various conditions, thereby revealing the optimal performance and associated parameters.

Figure 1 depicts the geometric configuration of the Nernst-based thermionic engine, which comprises a circular two-dimensional central region positioned perpendicular to a uniform magnetic field with a magnitude of B . The central region possesses a radius of R and is surrounded by four distinct thermochemical reservoirs. Electrons in reservoir C_i is characterized by the chemical potential μ_i and temperature T_i . Each of these reservoirs encompasses a segment of length l , which is equal to $\pi R/2$.

When an electron reaches the circular boundary from one of the reservoirs, it is assumed to enter the central region, where it undergoes a circular trajectory due to the influence of the Lorentz force. The average number of electrons with the range $(p_r, p_r + dp_r)$ of radial momentum and $(p_s, p_s + dp_s)$ of tangential momentum, located in a small area $drds$ at the boundary of reservoir C_i , is expressed as follows

$$dN_i \equiv 2 \exp[-\beta_i(E - \mu_i)] drdsdp_r dp_s / h^2, \quad (1)$$

where the approximation of Maxwell-Boltzmann statistics has been applied. Here, 2 denotes the spin of the electron, r represents the radial coordinate, and $E =$

* The two authors contributed equally to this work.

† sushanhe@xmu.edu.cn

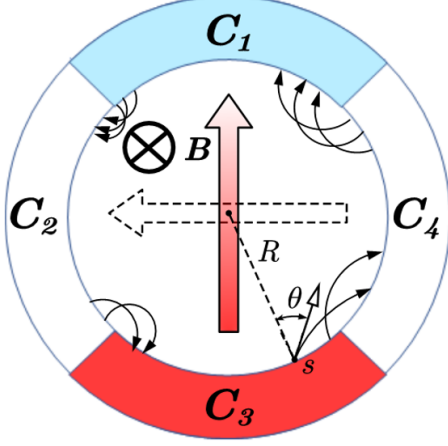


Figure 1. The scheme diagram of a Nernst-based thermionic engine. Reservoir C_3 possesses a higher temperature compared to reservoir C_1 ($T_3 > T_1$), while reservoir C_2 has a higher chemical potential than reservoir C_4 ($\mu_2 > \mu_4$). The red gradient arrow represents the flow of heat current, while dashed arrow represents the movement direction of particles. The circular arrow denote a typical trajectory for an electron under a strong magnetic field B . For example, an electron may leave reservoir C_3 at the position s with an angle θ and transports to reservoir C_4 .

$(p_r^2 + p_s^2)/(2m)$ is the kinetic energy of the electrons with m being the mass of electron, h is Planck's constant, and $\beta_i = 1/(k_B T_i)$ with k_B being Boltzmann's constant. For $p_r < 0$, any particle that contributes to dN_i will reach the boundary within the time interval $dt = -m dr/p_r$. Through the elimination of dr in favor of dt and the application of a change of variables $p_r = -\sqrt{2mE} \cos \theta$ and $p_s = \sqrt{2mE} \sin \theta$, we can express Eq. (1) in a different form. This change of variables leads to the relation

$$dN_i/dt = \frac{2\sqrt{2mE}}{h^2} \exp[-\beta_i(E - \mu_i)] \cos(\theta) ds dE d\theta. \quad (2)$$

By integrating over variables s , E , and θ , the total electron current J_i^+ flowing from the reservoir C_i into the central region is given by

$$\begin{aligned} J_i^+ &= 2 \int_l ds \int_0^\infty dE \int_{-\pi/2}^{\pi/2} d\theta \cos(\theta) u_i(E) \\ &= \frac{2\sqrt{2\pi m l}}{h^2 \beta_i^{3/2}} e^{\beta_i \mu_i}, \end{aligned} \quad (3)$$

where $u_i(E) = \sqrt{2mE} \exp[-\beta_i(E - \mu_i)]/h^2$.

By assuming that each electron reaching the boundary from the central region is absorbed in the adjacent reservoir, the expression for the steady-state current J_i^- flowing into C_i is calculated as follows

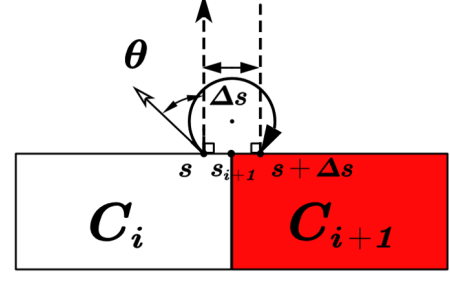


Figure 2. The trajectory of an electron starts at reservoir C_i from position s with an angle θ , and enters reservoir C_{i+1} at position $s + \Delta s$.

$$J_i^- = 2 \sum_j \int_l ds \int_0^\infty dE \int_{-\pi/2}^{\pi/2} d\theta u_j(E) \cos \theta \tau_i(E, s, \theta), \quad (4)$$

where $\tau_i(E, s, \theta)$ is the conditional probability for an electron with energy E that enters at position s with an angle θ and reaches the boundary of reservoir C_i after traversing the central region. In the context of purely Hamiltonian dynamics, this probability equals either 1 or 0 [23]. For the purpose of reaching a concise expression for the net current $J_i \equiv J_i^+ - J_i^-$ leaving reservoir C_i , the transmission coefficient

$$T_{ji}(E) \equiv \int_l ds \int_{-\pi/2}^{\pi/2} d\theta \tau_j(E, s, \theta) \cos \theta \quad (5)$$

is introduced.

From the volume-preserving property of Hamiltonian dynamics and the Poincaré-Cartan theorem, it can be demonstrated that [23]

$$\sum_i T_{ji}(E) = \sum_j T_{ji}(E) = 2l. \quad (6)$$

By combining (3), (4), and (6), the net current out of reservoir C_i

$$J_i = 2 \sum_j \int_0^\infty dE T_{ij}(E) [u_i(E) - u_j(E)]. \quad (7)$$

In a similar manner, the net heat flux leaving reservoir C_i is calculated by

$$Q_i = 2 \sum_j \int_0^\infty dE T_{ij}(E) (E - \mu_i) [u_i(E) - u_j(E)]. \quad (8)$$

The entropy production rate of the engine at steady state is expressed as

$$\dot{S} \equiv \sum_i Q_i/T_i. \quad (9)$$

To ensure thermodynamic consistency, \dot{S} must be non-negative.

For a Nernst engine, reservoir C_3 possesses a higher temperature compared to reservoir C_1 ($T_3 > T_1$), while reservoir C_2 has a higher chemical potential than reservoir C_4 ($\mu_2 > \mu_4$). Simultaneously, the constraint equations

$$J_1 = J_3 = 0 \quad \text{and} \quad Q_2 = Q_4 = 0, \quad (10)$$

are required. These conditions ensure that electron current only occurs horizontally and heat flow only takes place vertically, as depicted in Figure 1.

In the following steps, we will explicitly calculate the transmission coefficients $T_{ij}(E)$ under the influence of a strong magnetic field. An electron of energy E moves in a circular trajectory inside the central region with a radius

$$r(E) = \sqrt{2mE}/(eB) \quad (11)$$

because of the Lorentz force. After traveling a distance Δs along the boundary (as shown in Fig. 2), the electron eventually collides with the boundary. In the strong field limit, the radius $r(E)$ of the electron trajectory is

significantly smaller compared to the radius of the central region. Mathematically, we have $r(E) \ll R$ for the majority of electrons. As a result, the boundary can be approximated as a straight line, as illustrated in Fig. 2. The geometric analysis demonstrates that

$$\Delta s = 2r(E) \cos \theta. \quad (12)$$

Since $\Delta s \ll R$, electrons emitted from reservoir C_i will either pass to the adjacent reservoir C_{i+1} or return to C_i . In other words, electron transmission only occurs between neighboring reservoirs. Therefore, the transmission coefficient $T_{ji}(E) = 0$ for $j \neq i, i+1$. By applying the sum rules given in Eq. (6), it is recognized that $T_{ii}(E) = 2l - T_{(i+1)i}(E)$. Therefore, we are now tasked with calculating the transmission coefficient $T_{(i+1)i}(E)$ for the transition from reservoir C_i to C_{i+1} . To determine $T_{(i+1)i}(E)$, one should refer to Fig. 2 and observe that a electron injected from reservoir C_i at a specific position s can reach reservoir C_{i+1} only if $\Delta s \geq s_i - s$, where s_i denotes the contact point between reservoir C_i and C_{i+1} . By utilizing Eq. (12), this transmission condition is then given by $\theta_- < \theta < \theta_+$, where $\theta_{\pm} = \pm \arccos[(s_i - s)/(2r(E))]$. Finally, Eq. (5) can be rewritten as

$$T_{(i+1)i}(E) = \int_{s_i - 2r(E)}^{s_i} ds \int_{\theta_-}^{\theta_+} d\theta \cos \theta = \pi r(E). \quad (13)$$

In the meanwhile, the coefficient

$$T_{ii}(E) = 2l - \pi r(E) = \pi[R - r(E)]. \quad (14)$$

By combining Eqs. (4), (6), (13), and (14), the analytical solution of the steady-state current J_i^- flowing into C_i is calculated as follows

$$\begin{aligned} J_i^- &= 2 \int_0^\infty u_i(E) \pi [R - r(E)] dE + 2 \int_0^\infty u_{i-1}(E) \pi r(E) dE \\ &= \frac{\sqrt{2\pi m \pi R} e^{\beta_i \mu_i}}{h^2 \beta_i^{3/2}} - \frac{4\pi m e^{\beta_i \mu_i}}{e B h^2 \beta_i^2} + \frac{4\pi m e^{\beta_{i-1} \mu_{i-1}}}{e B h^2 \beta_{i-1}^2}. \end{aligned} \quad (15)$$

Equations (3), (7), and (15) yield the net current out of reservoir C_i

$$J_i = \frac{4\pi m e^{\beta_i \mu_i}}{e B h^2 \beta_i^2} - \frac{4\pi m e^{\beta_{i-1} \mu_{i-1}}}{e B h^2 \beta_{i-1}^2}. \quad (16)$$

Through an analogous calculation, the net heat flux leaving reservoir C_i in Eq. (8) is simplified as

$$Q_i = \frac{8\pi m e^{\beta_i \mu_i}}{e B h^2 \beta_i^3} - \frac{8\pi m e^{\beta_{i-1} \mu_{i-1}}}{e B h^2 \beta_{i-1}^3} - \mu_i \frac{4\pi m e^{\beta_i \mu_i}}{e B h^2 \beta_i^2} + \mu_{i-1} \frac{4\pi m e^{\beta_{i-1} \mu_{i-1}}}{e B h^2 \beta_{i-1}^2}. \quad (17)$$

In the aforementioned circumstances, a noticeable movement of electrons only occurs between C_2 and C_4 , whereas the net flow of heat is solely observed from C_3

to C_1 . The spontaneous directed flow of heat leads to the migration of electrons from the reservoir with lower chemical potential to the reservoir with higher chemical

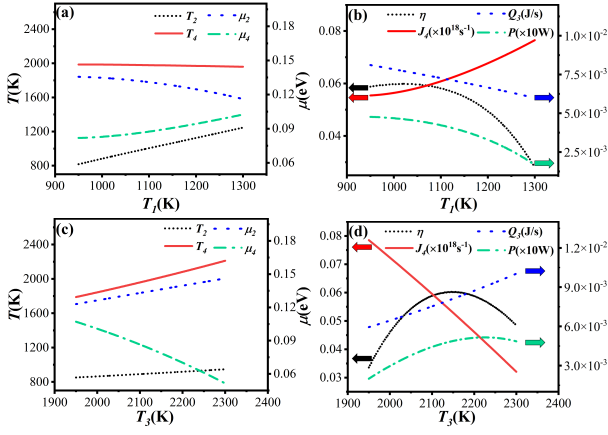


Figure 3. (a) The dependence of parameters T_2 , T_4 , μ_2 and μ_4 of reservoir C_2 and C_4 , and (b) the efficiency η , power P , current J_4 , and heat flux Q_3 on the temperature T_1 of reservoir C_1 , where the temperature $T_3=2121K$. (c) The dependence of parameters T_2 , T_4 , μ_2 and μ_4 of reservoir C_2 and C_4 , and (d) the efficiency η , power P , current J_4 , and heat flux Q_3 on the temperature T_3 of reservoir C_3 , where the temperature $T_1=1012K$. The other parameters $\mu_1 = 0.16eV$, $\mu_3 = 0.003eV$, $R = 1m$, and $B = 1T$. The arrows in Figs. (b) and (d) indicate the values of the corresponding physical quantities, which are shown in the same color.

potential. The power output of the engine is defined as

$$P = (\mu_2 - \mu_4) J_4, \quad (18)$$

while the energy conversion efficiency is given by

$$\eta = (\mu_2 - \mu_4) J_4 / Q_3. \quad (19)$$

The parameters T_2 , T_4 , μ_2 and μ_4 of reservoir C_2 and C_4 can be determined by utilizing the constraint equations given in Eq. (10). Figure 3(a) reveals that the temperature T_4 of reservoir C_4 remains approximately constant at around 2000K. As T_1 increases, T_4 shows a slight downward trend, while the temperature T_2 of reservoir C_2 exhibits a slightly steeper upward trend. The behaviors of μ_2 and μ_4 are quite contrasting, where μ_2 decreases and μ_4 increases with the increase of T_1 . Figure 3(b) shows that the efficiency η reaches a peak value of 5.98% at $T_1 = 1023.6K$. As T_1 increases, both the power P and the heat flux Q_3 heat experiences a decline.

According to the expressions in Eqs. (16) and (17), the constraint equations $J_1 = 0$ and $Q_4 = 0$ can be derived

$$T_1^2 e^{\beta_1 \mu_1} = T_4^2 e^{\beta_4 \mu_4}, \quad (20)$$

$$(2T_4^3 k_B - \mu_4 T_4^2) e^{\beta_4 \mu_4} = (2T_3^3 k_B - \mu_3 T_3^2) e^{\beta_3 \mu_3}. \quad (21)$$

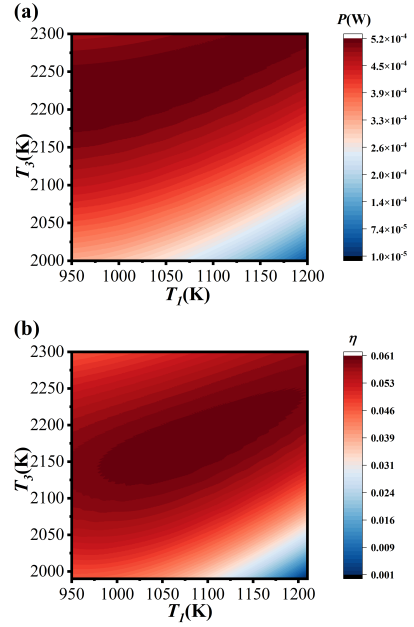


Figure 4. The two-dimensional graph of (a) the power P and (b) efficiency η varying with T_1 and T_3 , while keeping the other parameters the same as those used in Fig. 3.

When μ_1 is a given value, the left-hand side of Eq. (20) is only a function of T_1 . By taking its derivative, it can be found that within the selected temperature range of T_1 , the derivative of the left-hand side of Eq. (20) is greater than 0. Due to the constraint $J_1 = 0$, the value of the right-hand side of Eq. (20) also needs to be increased accordingly as T_1 increases. Therefore, μ_4 increases with the increase of T_1 in Fig. 3(a). Since the values of T_3 and μ_3 are both given, the right-hand side of Eq. (21) is a fixed value. Dividing Eq. (21) by Eq. (20), we can get

$$2T_4 k_B - \mu_4 = \frac{(2T_3^3 k_B - \mu_3 T_3^2) e^{\beta_3 \mu_3}}{T_1^2 e^{\beta_1 \mu_1}}. \quad (22)$$

It can be seen that left-hand side of Eq. (22) should decrease with the increase of T_1 for the condition $Q_4 = 0$. In Fig. 3(a), the decrease of T_4 and the increase of μ_4 reflect this process. Using the same analysis, we can obtain the changes in T_2 and μ_2 . As shown in Fig. 3(a), the difference between μ_2 and μ_4 is a decreasing function of T_1 . For the Nernst heat engine, this trend reduces the efficiency. However, the increase of J_4 and the decrease of Q_3 shown in Fig. 3(b) serve to increase the efficiency of the heat engine. For these two reasons, the efficiency of the heat engine will reach an extreme value.

The above analysis can also be applied to reveal the dependence of parameters T_2 , T_4 , μ_2 and μ_4 of reservoir C_2 and C_4 on the temperature T_3 in Fig. 3 (c), as well as the dependence of the efficiency η , power P , current J_4 , and heat flux Q_3 on the temperature T_3 in Fig. 3(d).

The relationship between the power P and efficiency η in relation to temperatures T_1 and T_3 is illustrated in

Figure 4(a). When the given value of T_3 is small, P decreases significantly as T_1 increases. However, when the given value of T_3 is large, P starts to increase as T_1 increases. When T_1 is held at a constant value, the power P exhibits an extremum as T_3 varies. Figure 4(b) depicts a region where the efficiency reaches its maximum value as both T_1 and T_3 vary. Optimal performance, characterized by enhanced power and efficiency, is attained when both temperatures fall within the dark red area of the contour plot.

In this work, we perform numerical simulations on a Nernst-based thermionic engine. By specifying the temperature and chemical potential of certain heat sources, we calculate the resulting changes in temperature and

chemical potential of unknown heat reservoirs. Moreover, we determine the system's power output and the heat flux that drives the system. Surprisingly, we discover that by determining the temperature or chemical potential of C_1 and C_3 and optimizing the remaining parameters, we can achieve the maximum power and efficiency of the Nernst heat engine. This discovery highlights the practicality of optimizing the performance of the Nernst heat engine.

This work has been supported by the National Natural Science Foundation (12075197 and 12364008), Natural Science Foundation of Fujian Province (2023J01006), Educational Teaching Reform Research Project of University Physics Discipline Alliance of Fujian Province (FJPHYS-2023-A02), and Fundamental Research Fund for the Central Universities (20720240145).

-
- [1] H. Goldsmid, *Introduction to thermoelectricity*, Vol. 121 (Springer, 2010).
- [2] K. Behnia and H. Aubin, *Reports on Progress in Physics* **79**, 046502 (2016).
- [3] T. Chiang, J. Nordlander, J. A. Mundy, and J. T. Heron, *Applied Physics Letters* **124**, 152404 (2024).
- [4] P. J. Price, *Phys. Rev* **102**, 1245 (1956).
- [5] S. J. Silverman, R. O. Carlson, and H. Ehrenreich, *Journal of Applied Physics* **34**, 456 (1963).
- [6] S. J. Watzman, T. M. McCormick, C. Shekhar, S.-C. Wu, Y. Sun, A. Prakash, C. Felser, N. Trivedi, and J. P. Heremans, *Physical Review B* **97**, 161404 (2018).
- [7] M. Murata, K. Nagase, K. Aoyama, and A. Yamamoto, *Applied Physics Letters* **117**, 103903 (2020).
- [8] R. Masuki, T. Nomoto, and R. Arita, *Physical Review B* **103**, L041202 (2021).
- [9] B. Sothmann, R. Sánchez, and A. N. Jordan, *Europhysics Letters* **107**, 47003 (2014).
- [10] J. G. Checkelsky and N. P. Ong, *Physical Review B* **80**, 081413 (2009).
- [11] D. L. Bergman and V. Oganesyan, *Physical Review Letters* **104**, 066601 (2010).
- [12] S. G. Sharapov, A. A. Varlamov, C. Goupil, and A. V. Kavokin, *Physical Review Research* **3**, 013140 (2021).
- [13] S.-G. Cheng, Y. Xing, Q.-F. Sun, and X. C. Xie, *Physical Review B* **78**, 045302 (2008).
- [14] H. Yang, W. You, J. Wang, J. Huang, C. Xi, X. Xu, C. Cao, M. Tian, Z.-A. Xu, J. Dai, and Y. Li, *Physical Review Materials* **4**, 024202 (2020).
- [15] A. Sakai, Y. P. Mizuta, A. A. Nugroho, R. Sihombing, T. Koretsune, M.-T. Suzuki, N. Takemori, R. Ishii, D. Nishio-Hamane, R. Arita, P. Goswami, and S. Nakatsuji, *Nature Physics* **14**, 1119 (2018).
- [16] F. Caglieris, C. Wuttke, S. Sykora, V. Süß, C. Shekhar, C. Felser, B. Büchner, and C. Hess, *Physical Review B* **98**, 201107 (2018).
- [17] M. Ikhlas, T. Tomita, T. Koretsune, M.-T. Suzuki, D. Nishio-Hamane, R. Arita, Y. Otani, and S. Nakatsuji, *Nature Physics* **13**, 1085 (2017).
- [18] K. Tang, Y. Yang, J. Shen, M. Shi, N. Zhang, H. Li, H. Li, Z. Liu, D. Shen, R. Wang, Y. Gao, J. He, Z. Xiang, and X. Chen, *Communications Materials* **5**, 89 (2024).
- [19] S. Kurosawa, T. Higo, S. Saito, R. Uesugi, and S. Nakatsuji, *Physical Review Materials* **8**, 054206 (2024).
- [20] K. Brandner and U. Seifert, *New Journal of Physics* **15**, 105003 (2013).
- [21] K. Brandner, K. Saito, and U. Seifert, *Physical Review Letters* **110**, 070603 (2013).
- [22] M. Murata, T. Hirai, T. Seki, and K. Uchida, *Applied Physics Letters* **124**, 193901 (2024).
- [23] J. Stark, K. Brandner, K. Saito, and U. Seifert, *Physical Review Letters* **112**, 140601 (2014).
- [24] K. Brandner (2015).
- [25] H. M. Pastawski, *Physical Review B* **44**, 6329 (1991).